THE JOURNAL OF PHYSICAL CHEMISTRY Letters

Letter

pubs.acs.org/JPCL

Quantum Yield of Polariton Emission from Hybrid Light-Matter States

Shaojun Wang, Thibault Chervy, Jino George, James A. Hutchison, Cyriaque Genet, and Thomas W. Ebbesen*

ISIS & icFRC, Université de Strasbourg and CNRS (UMR 7006), 8 allée Gaspard Monge, Strasbourg 67000, France

Supporting Information

ABSTRACT: The efficiency of light-matter strong coupling is tuned by precisely varying the spatial position of a thin layer of cyanine dye J-aggregates in Fabry–Perot microcavities, and their photophysical properties are determined. Placing the layer at the cavity field maximum affords an interaction energy (Rabi splitting) of 503 meV, a 62% increase over that observed if the aggregates are simply spread evenly through the cavity, placing the system in the ultrastrong coupling regime. The fluorescence quantum yield of the lowest polaritonic state P− integrated over k-space is found to be ~10^{-2}. The same value can be deduced from the 1.4 ps lifetime of P− measured by femtosecond transient absorption spectroscopy and the calculated radiative decay rate constant. Thus, the polariton decay is dominated by nonradiative processes, in contrast with what might be expected from the small effective mass of the polaritons. These findings provide a deeper understanding of hybrid light-molecule states and have implications for the modification of molecular and material properties by strong coupling.

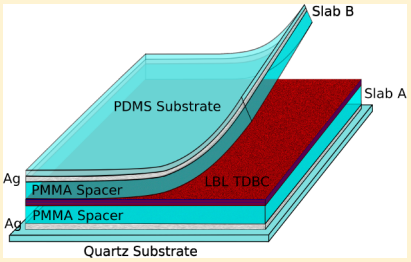

SECTION: Plasmonics, Optical Materials, and Hard Matter

The strong coupling of organic materials with light results in the formation of hybrid light-matter states with unique optical and electronic properties, stimulating growing interest from physics to molecular science.[1−28] The presence of the hybrid states has been shown to modify relaxation pathways,[6,7,15,18,21] photochemical reaction rates,[12] the work function of organic materials,[16] and the energy of the ground state of the coupled system.[17] Significantly, the bosonic character of these hybrid states has been employed to achieve collective effects such as polariton lasing and Bose–Einstein condensation at room temperature.[8,9]

The hybrid states are formed when photons are exchanged between a material and a resonant optical cavity mode at a rate faster than their respective dephasing processes. This back-and-forth exchange, Rabi oscillation, leads to a quantum superposition of the uncoupled molecular transition and the optical resonance, resulting in the generation of two new eigenstates for the system, the upper P+ and lower P− polaritonic states, separated by the Rabi-splitting $\hbar\Omega_R$ (see Figure 1a). The strong coupling can be illustrated by placing J-aggregates of a cyanine (TDBC), having a maximum absorption at 588 nm (Figure 1b), inside a resonant Fabry–Perot cavity, as illustrated in Figure 1c. The transmission spectrum is strongly modified with two new peaks separated in this case by a Rabi splitting of 325 meV.

Theory predicts that the Rabi splitting ($\hbar\Omega_R$) is proportional to the scalar product of the electromagnetic field amplitude ($\vec{E}$) at the energy $\hbar\omega$ of the optical resonance and the material transition dipole moment ($\vec{d}$), which in the absence of dissipation is given by

$$\hbar\Omega_R = 2\vec{E}\cdot\vec{d} \times \sqrt{n_{ph}+1} = 2\sqrt{\frac{\hbar\omega}{2\varepsilon_0 V}}\, d \times \sqrt{n_{ph}+1} \quad (1)$$

where ε_0 is the vacuum permittivity and n_{ph} is the number of photons involved in the coupling process. An important feature of eq 1 is that the splitting can still occur even in the absence of real photons ($n_{ph} = 0$) due to the interaction of the molecular transition dipole and the cavity mode through zero-point energy fluctuations. This residual splitting is known as the vacuum Rabi splitting ($\hbar\Omega_{VR}$). All experiments reported here are done in this regime. Furthermore, the Rabi-splitting increases as the square root of the molecular concentration C because $\hbar\Omega_{VR} \propto (N/V)^{1/2} = \sqrt{C}$, where N is the number of coupled molecules in the mode volume V.[20]

Organic dyes are particularly well-suited for strong coupling due to their large transition dipole moment. Working at high molecular concentrations, the Rabi splitting can approach 1 eV, representing a substantial fraction of the molecular transition energy and reaching the so-called ultrastrong coupling regime, where the energy levels are significantly perturbed.[11,17] This regime can be reached even for low-Q resonances (ca. 10 to 20) as long as Rabi splitting is large.

Received: March 2, 2014
Accepted: April 2, 2014
Published: April 2, 2014

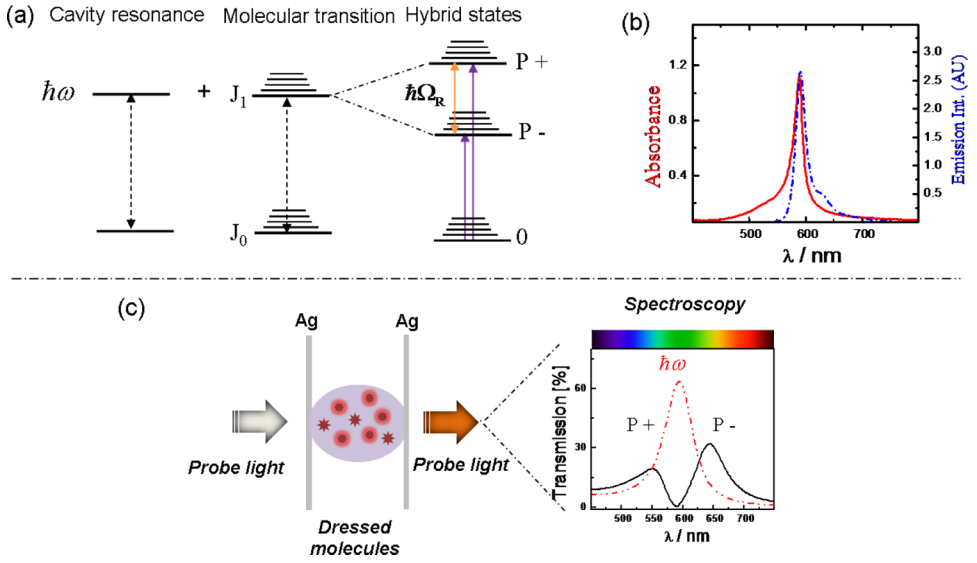

Figure 1. (a) Schematic representation of the coupling of a molecular transition (J_0-J_1) and an optical resonance of energy ($\hbar\omega$) forming the hybrid states P+ and P− separated by the Rabi splitting energy ($\hbar\Omega_R$). (b) Absorption (red solid line) and emission spectrum (blue dashed line) of J-aggregate layer of TDBC (5,6-dichloro-2-[[5,6-dichloro-1-ethyl-3-(4-sulphobutyl)benzimidazol-2-ylidene]propenyl]-1-ethyl-3-(4-sulphobutyl) benzimidazolium hydroxide). (c) Schematic illustration of TDBC dispersed in the $\lambda/2$ Fabry−Perot (FP) cavity everywhere. Transmission spectra of the bare cavity (red) and in the presence of dispersed TDBC in resonance with the cavity giving rise to P+ and P−.

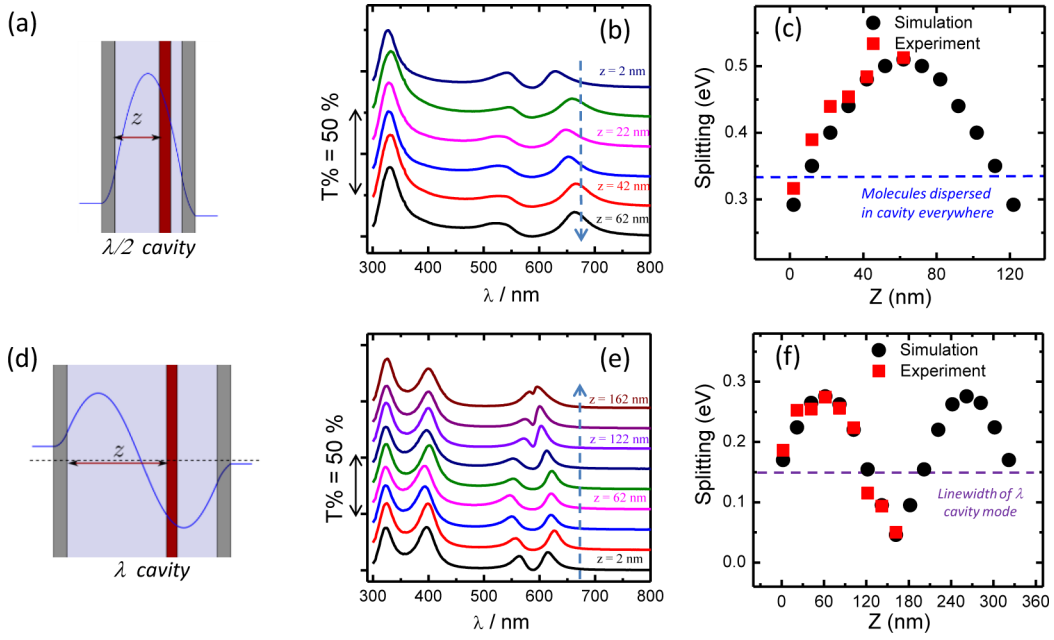

Figure 2. (a) Schematic representation of the $\lambda/2$ cavity and the corresponding field amplitude. (b) Transmission spectra of a set of $\lambda/2$ cavities resonant with a TDBC molecular layer located at different spatial positions inside the cavity (z from the edge to center as indicated by the dashed blue arrow and every spectrum is offset in T% by 18%). These spectra were measured under 35° incidental angle and TE polarization. (c) Rabi splitting versus spatial position of the molecular layers inside the $\lambda/2$ mode cavities. (Blue dashed line represents the $\hbar\Omega_{VR}$ when the molecules are dispersed evenly inside the cavity.) (d) Schematic representation of the λ cavity and the corresponding field amplitude. (e) Normal incidence transmission spectra of a set of λ mode cavities with TDBC molecular layer and (f) their corresponding $\hbar\Omega_{VR}$ (red squares) at different spatial positions inside the cavity. The purple dashed line indicates the fwhm line-width of the λ mode (150 meV) as the minimum energy splitting below which strong coupling can no longer be defined. Black dots in panels c and f are the calculated splittings using the transfer matrix simulation, where the complex refractive index of the TDBC J-aggregate film was extracted from its absorption spectrum via a Kramers−Kronig transformation and the thicknesses of the Ag mirrors and PMMA spacer layers were taken from experiments.

Here we investigate further fundamental aspects of light-molecule strong coupling, such as the quantum yield of polariton emission, which as far as we know has never been reported, and the implication on the decay mechanism of the coupled state. We study these features as a function of the Rabi splitting and the location of the molecules relative to the optical mode (illustrated in Figure 2a,d). From eqs 1 and 2, we expect that the Rabi splitting is at a maximum when molecules are placed at the antinodes of the optical field

dx.doi.org/10.1021/jz5004439 | J. Phys. Chem. Lett. 2014, 5, 1433−1439

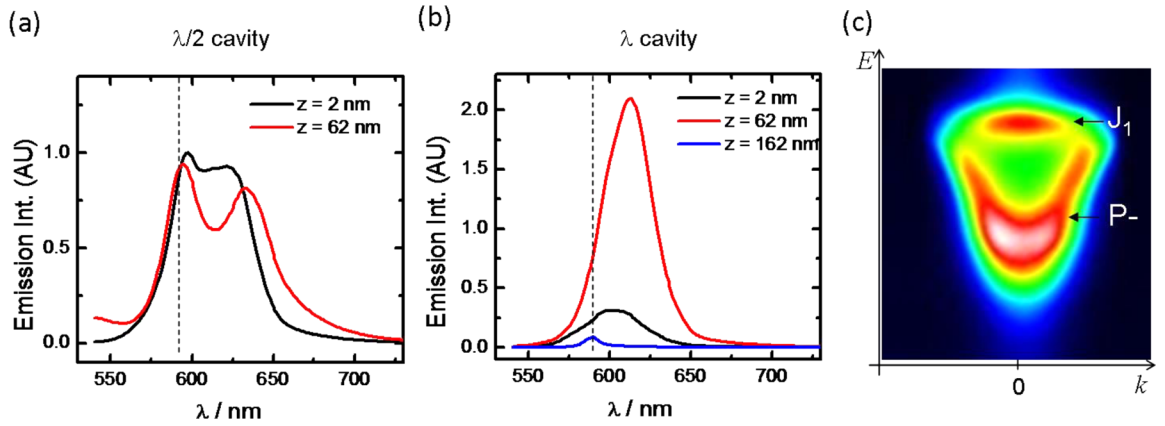

Figure 3. Fluorescence emission spectra (collected normal to the sample plane, excitation wavelength 520 nm) of (a) $\lambda/2$ mode cavities with TDBC molecular layer in two different spatial positions of the cavity (z: 2 and 62 nm) and (b) λ mode cavities with three different spatial positions of the cavity (z: 2, 62, 162 nm). The dashed vertical line in the spectra indicates the maximum of the fluorescence of J_1 of uncoupled J-aggregates. The peaks to the right are due to the fluorescence of P−. (c) Example of the dispersion of the P− fluorescence collected over k-space.

modes where E is strongest, and this should be optimal for the smallest mode volume V.

As detailed in the sample fabrication, we have developed a method to precisely locate a highly absorbing, thin (~25 nm) film of a cyanine J-aggregate in a Fabry−Perot (FP) cavity, varying its position in ~10 nm steps from the edge to the center of the cavity (Figure 2). This allows us to quantitatively analyze the strong coupling interaction strength as a function of molecular spatial position inside the cavity with much higher resolution than had been achieved previously for organic systems.[4] The spatial distribution of the optical field amplitude E in the cavity for the $\lambda/2$ and λ FP modes is indicated schematically in Figure 2a,d, respectively.

In Figure 2b are shown transmission spectra for the $\lambda/2$ FP cavity in resonance with the J-aggregate, when the molecular film of the same absorbance as in Figure 1b is moved gradually from the edge of one of the silver mirrors to the center of the cavity. The Rabi-splitting increases from 310 to 503 meV for this sequence (Figure 2b), following the predicted spatial distribution of the optical field amplitude for the mode, as simulated using Maxwell's equations (compare Figure 2a,c). Indeed, the observed $\hbar\Omega_{VR}$ can be reproduced by inserting the complex refractive indices of the various cavity component layers into Maxwell's equations in the "classical" limit and employing transfer matrix formalism (Figure 2c).[11,29]

When the J-aggregate film is at the center of the $\lambda/2$ cavity (the field antinode), the Rabi splitting is 1.54 times higher than if the same optical density of J-aggregate is dispersed throughout the whole cavity (dashed blue line, Figure 2c). This is further confirmed by the angle-dependent dispersion properties of the cavity in which the molecular layer is positioned at the field maximum (Supplementary Figure S1b in the Supporting Information). An important point to note for coupling to the $\lambda/2$ FP mode is that even when the molecular layer is at the edge of the cavity the system remains in the strong coupling regime. (That is, $\hbar\Omega_{VR}$ is greater than the line width of the $\lambda/2$ FP mode (210 meV) and the fwhm of the J-aggregate band at 588 nm (72 meV).)

In the next set of experiments, we increased the thickness of the FP cavities to 350 nm, such that the λ FP mode was resonant with the 588 nm absorption band of the J-aggregate (Figure 2d−f). Again, the 25 nm thick TDBC layer was moved from the center of the cavity (z = 162 nm) to the edge (z = 2 nm). The observed Rabi splitting is at a maximum (280 meV) when the molecular film is at a quarter of the cavity (z = 62 nm), whereas it reduced to 190 meV for molecules at the edge of the cavity and to just 40 meV when the molecules are at the center. Again, this corresponds to the expected spatial distribution of the λ FP cavity mode amplitude and closely agrees with transfer matrix simulations. It is interesting to note that $\hbar\Omega_{VR}$ is ~1.58 higher for the $\lambda/2$ cavity than for the λ cavity when the molecular layer is placed at field antinode of these cavities. This observation is in quantitative agreement with the dependence of the Rabi splitting on the mode volume as predicted by eq 1 ($\hbar\Omega_{VR}^{\lambda/2}/\hbar\Omega_{VR}^{\lambda} \propto (V_\lambda/V_{\lambda/2})^{1/2} = 1.60$), the two different mode volumes being estimated by the transfer matrix method.

The dashed blue line in Figure 2f is the Rabi splitting energy threshold, above which the system can be defined to be in the strong coupling regime (125 ± 25 meV). Thus, by moving the position of the molecular layer from the quarter of the cavity to the center, the λ cavity can be tuned from weak to strong coupling regime, which is very valuable for elucidating cavity effects, as we present later.

Figure 3 compares the emission spectra of the molecular film placed at the field nodes and antinodes in the $\lambda/2$ and λ cavities. Fluorescence spectra of such coupled systems typically exhibit two components: one corresponding to uncoupled molecules from J_1 and the other to those from P− state.[15,18] Furthermore, emission from P+ is rarely observed, which is attributed to rapid nonradiative decay to the lower energy levels at room temperature.[15,18] This is certainly the case here for the $\lambda/2$ cavity, where emission peaks from both uncoupled molecules and P− can be observed whether the J-aggegate film is placed at the center (antinode) or at the edge (node) of the cavity (Figure 3a). Note that, as expected, the P− emission moves to longer wavelengths with the higher coupling strength at the antinode (z = 62 nm).

In the case of the λ cavity, only the fluorescence from the uncoupled excited state J_1 is observed (blue curve, Figure 3b) when the J-aggregate film is placed at the center of the cavity (the central node, z = 162 nm). In contrast, the polariton

dx.doi.org/10.1021/jz5004439 | J. Phys. Chem. Lett. 2014, 5, 1433−1439

emission dominates (red curve, Figure 3b) when the molecular films are at the antinode of the cavity (z = 62 nm). Finally, at the edge of the λ cavity (z = 2 nm), the emission from both states overlaps.

The fluorescence quantum yield (Φ_f) gives insight into the relaxation pathways in strongly coupled molecular system because

$$\Phi_f = \frac{k_r}{k_r + k_{nr}} = \tau \cdot k_r \tag{2}$$

where k_r and k_{nr} are the radiative and nonradiative decay rates and τ is the lifetime of the emitting state. We measured the Φ_f values of the coupled system and that of a bare TDBC film outside the cavity. (See the Supporting Information for details.) The $\Phi_f(J_1)$ of the bare film was found to be 0.02. Because the cavity emission properties are dispersive (angle-dependent), as shown in Figure 3c, the measurement of Φ_f of P− requires careful integration over all angles, as described in Supporting Information, together with the deconvolution of the contributions of P− and J_1. When the J-aggregate layer is at the antinode in the $\lambda/2$ cavity, $\Phi_f(P-) \approx 8 \times 10^{-3}$, while it is slightly higher (10^{-2}) at the antinode of the λ cavity. In contrast, at the center of the λ cavity where only J_1 emits, $\Phi_f(J_1) = 10^{-3}$. This 20-fold suppression of the radiative rate of J_1 at the center of the λ cavity as compared with the bare film, is due to a Purcell effect because the electromagnetic field is extremely weak at the node. It is important to note that such suppression is observed because of the small Stoke shift, which implies that the emission overlaps with the cavity mode. Table 1 summarizes the main findings in regards to the quantum yields and the radiative and nonradiative rates under these different conditions.

Table 1. Experimental Results of Different Samples

	J_1 of bare film	P− of $\lambda/2$ cavity antinode	J_1 of λ cavity node	P− of λ cavity antinode
$\tau_{1/2}$ (ps)	0.6	1.4	0.6	1.4
Φ_f	2×10^{-2}	8×10^{-3}	1×10^{-3}	1×10^{-2}
k_r (s^{-1})	3×10^{10}	5.7×10^{9}	1.7×10^{9}	7.1×10^{9}
k_{nr}(s^{-1})	1.6×10^{12}	7.1×10^{11}	1.7×10^{12}	7.1×10^{11}

The very low Φ_f values confirm that nonradiative relaxation is the dominant decay pathway in both coupled systems and the bare TDBC with $k_{nr} \approx 10^{12}$ $s^{-1} > 100k_r$. (See Table 1.) This is due to the numerous molecular vibrational modes, which are available to redistribute the energy (ca. 180 fundamental modes in the case of TDBC), and also energy transfer to defects and perhaps dimers in the J-aggregates.[36,37]

Next, we undertook femtosecond transient absorption spectroscopy measurements by exciting at 585 nm, comparing the spectra and the decay dynamics outside the cavity with the data collected for different positions inside the cavity. Figure 4a,c shows the differential absorption spectra recorded for the λ cavity at the node (center) and the antinode, respectively. In the center the differential spectrum is that of the bare TDBC and decays with the same lifetime ($\tau_{1/2}$ = 0.6 ps) (Figure 4b), in agreement with the fact that the system is in the weak coupling regime.

At the antinode, the spectral shape (Figure 4c) is in agreement with those reported previously for strongly coupled TDBC systems.[7,15,21] However, at this location, the decay depends on the detection wavelength. At the region corresponding to the absorption of the uncoupled molecules (∼588 nm), the decay matches that measured outside the cavity ($\tau_{1/2}$ = 0.6 ps), but at the region corresponding to the P− absorption, the decay lifetime is longer ($\tau_{1/2}$ = 1.4 ps) (Figure 4d). It should be noted that the decay kinetics are not a true exponential, but we checked that they are independent of pump intensity in the range used even inside the cavity for the uncoupled TDBC. In the other words, the complex decay is due to intrinsic inhomogeneity in the sample.

In the $\lambda/2$ cavity, the transient spectra has features of the strongly coupled system and the decay kinetics ($\tau_{1/2}$ = 1.4 ps) is the same at all wavelengths, indicating that most of the TDBC molecules are coupled (Figure S4 in the Supporting Information). We summarized the experimental results of different samples in Table 1.

The previously measured lifetimes and Φ_f(P−) are related by k_r, as seen from eq 2. k_r of J-aggregates are is to be much larger than the monomer due to the extended exciton delocalized over ∼10 molecules. It can also be calculated from the absorption using Einstein's coefficients, as is typically done to estimate the radiative rates of organic molecules with the Bowen and Wokes equation[30]

$$k_r \approx 2.9 n^2 \bar{\nu}^2 \int \varepsilon \, d\nu \tag{3}$$

where n is the refractive index of the film, $\bar{\nu}$ is the central absorption frequency in inverse centimeters, and ε is the molar extinction coefficient. For TDBC, k_r is reported in the literature to be $\sim 4 \times 10^9$ s^{-1} in solution,[31] yielding $\Phi_f(J_1) \approx 2 \times 10^{-3}$, while if we calculate k_r from our experimentally determined absorption using eq 3, assuming the cross-section of 10 molecules, we find $k_r \approx 10^{10}$ s^{-1}, which gives $\Phi_f(J_1) \approx 6 \times 10^{-3}$. These values are in reasonable agreement considering all uncertainties.

For P−, we can also estimate k_r from eq 3, assuming that the oscillator strength is ultimately preserved in the coupled system of the two new transitions (P+ and P−). Measurement of the area under the absorption curve before and after coupling indicates that this is indeed the case. With this approach, we estimate $k_r \approx 0.5 \times 10^{10}$ s^{-1}, which, given a lifetime of 1.4 ps, yields Φ_f(P−) ∼7×10^{-3}. The magnitude of the order is in remarkable agreement with our measured values.

These results clearly indicate that the lifetime of the P− is much longer than the lifetime of the photon in the cavity (here 20 fs). This has been observed in previous cases,[5,7,15,21] but here the combination of precise positioning inside the cavity has allowed verification of this point beyond doubt. In the past, long-lived P− has been generally attributed to complex energy-transfer processes involving the weak/uncoupled molecular states, a form of delayed fluorescence.[32] The quantum yields and the transient dynamics presented here are mutually consistent and do not require the invocation of any such special mechanism. P− is thus intrinsically longer lived than its constituent states. This might seem surprising, but there are many examples of species whose lifetimes are longer than those of their components. In molecular science, the most notable are excimers formed from the coupling of excited molecule (M*) and another molecule in the ground state (M):

$$M^* + M \rightleftarrows (MM^*)$$

dx.doi.org/10.1021/jz5004439 | J. Phys. Chem. Lett. 2014, 5, 1433−1439

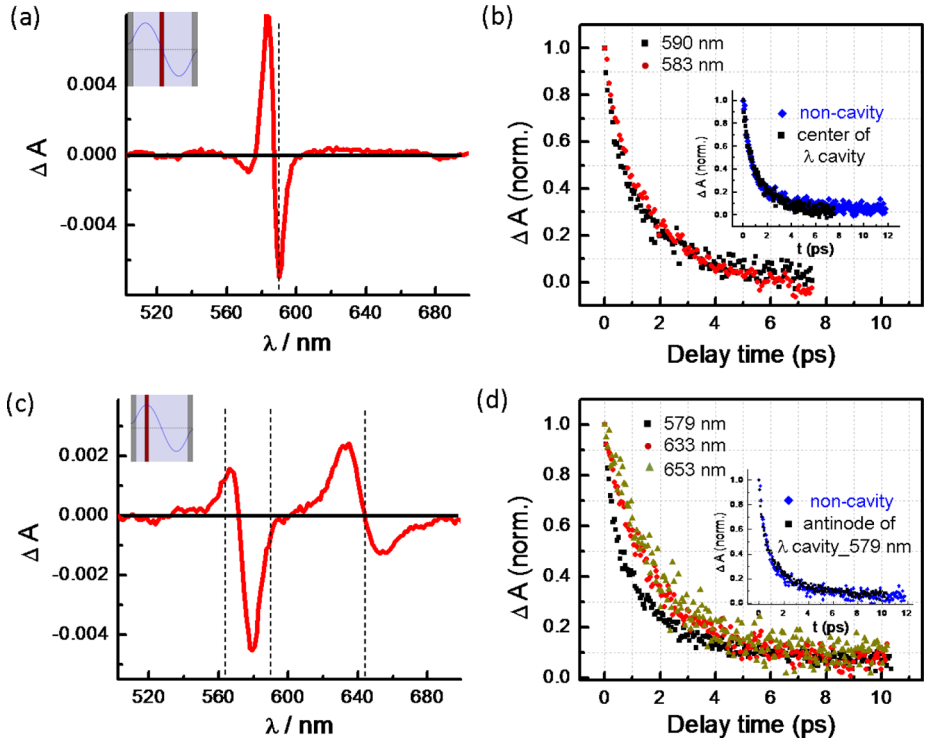

Figure 4. (a,c) Transient absorption spectra of TDBC layer in the center and at the antinode of λ mode cavity. The dashed vertical lines indicate the absorption maxima of the J-band of uncoupled molecules, P+ and P− in panel c. (b,d) Decay kinetics for the two spatial positions in (a) and (c) respectively, measured at different wavelengths. The insert in (b) show that the decay at the node of the cavity is identical to that of the TDBC layer in the absence of the top mirror (noncavity). The insert in (d) shows that the decay at 579 nm for a TDBC layer at the antinode is the same as that of TDBC in the absence of cavity (noncavity).

The excimer is stabilized by the coupling interaction, leading to cases where the lifetime of (MM*) is much longer than M*. For instance, excited naphthalene monomer has a lifetime of 52 ns at room temperature in ethanol, while its excimer has a lifetime of 380 ns.[30] Similarly, upon the formation of the exciplex between naphthalene diimide and toluene, the lifetime increases by an order of magnitude over the monomer.[33]

The lifetime of the hybrid light-matter states is going to be sensitive to the Rabi splitting and not necessarily longer than both the component states. In the Markovian regime, where the splitting is typically small relative to k_BT, the lifetime of the polaritonic states is similar and determined by the shortest of the states involved in the strong coupling. In the cases where the Rabi splitting is much larger than k_BT, the coupled system is in the non-Markovian regime, in which case the properties of P− and P+ cannot be predicted in any simple way.[19] Instead, these properties can only be determined theoretically in the coupled state ab initio. In the non-Markovian regime, P+ is always observed experimentally to be much shorter lived than P−, in a similar way to upper excited molecular states, due to rapid vibrational relaxation and other nonradiative decay processes. As we have shown here, P− lifetime can be relatively long, but it is also determined overwhelmingly by the very fast nonradiative relaxation processes ($k_{nr} \approx 10^{12}$ s^{-1}). Polariton fluorescence is thus a very minor decay path. On the fundamental side, this cautions against using only emission spectra to elucidate decay mechanisms. In addition, despite the fact that polaritons are quasi-bosons, strongly coupled molecular systems are in most cases uninteresting for making light-emitting devices unless the system is carefully chosen such as in the demonstration of polariton lasing.[8] Nevertheless, strongly coupled systems offer many exciting possibilities for modifying molecular and material properties with potential applications from chemistry to optoelectronics.

METHODS

Sample Fabrication. We developed a bonding technique for the precise control of the cyanine J-aggregate film's position in the Fabry−Perot microcavity. To begin, a 30 nm thick silver film was sputtered on a glass substrate, upon which was spin-coated a film of poly(methyl methacrylate) (PMMA) of variable thickness (labeled slab A). Meanwhile, a 30 nm thick silver film was evaporated on a 1.0 mm thick poly-(dimethylsiloxane) (PDMS) substrate upon which was spin-coated a layer of PMMA of variable thickness (labeled slab B). The surface of the PMMA on slab A was made hydrophilic by spin-coating a ∼2 nm thick PDMS layer on it (from 0.3 wt % in *tert*-butanol) and exposing it to an oxygen plasma for 30 s. Next, layers of J-aggregates of the cyanine TDBC (5,6-dichloro-2-[[5,6-dichloro-1-ethyl-3-(4-sulphobutyl)benzimidazol-2-ylidene]propenyl]-1-ethyl-3-(4-sulphobutyl) benzimidazolium hydroxide, inner salt, sodium salt, few Chemicals) and of the polycation poly-(diallyldimethylammonium chloride) (PDDA) solution (average M_w 200 000−350 000, 20 wt % in water, Aldrich) were alternately adsorbed onto the surface of slab A using layer-by-layer assembly.[34,35] Polyelectrolyte layers were deposited by soaking slab A for 5 min in a solution of PDDA (6×10^{-2} M) in deionized water. J-aggregate layers were deposited by soaking slab A for 5 min in a solution of TDBC (1×10^{-4}

dx.doi.org/10.1021/jz5004439 | J. Phys. Chem. Lett. 2014, 5, 1433−1439

M) in H_2O, which had been previously sonicated for 60 min at 35 °C. The surface of slab B was coated with a ∼2 nm thick film of PDMS. Finally, the polymer face of slab B was sealed to the molecular film surface of slab A to form a low-quality (Q factor ≈ 12) optical microcavity. By controlling the thickness of the PMMA layers on slab A and slab B, the position of the J-aggregate layer could be placed near the edge of the cavity or at the center of the cavity. The whole cavity length, including the PMMA and molecular films, could be tuned such that the J-aggregates absorption band at 588 nm was resonant with either the $\lambda/2$ or λ FP cavity mode. Film thicknesses were measured using Alpha-step IQ surface profilometer.

Steady-State Spectroscopy. Steady-state transmission and reflection spectra were taken on a Shimadzu UV3101 spectrometer. Steady-state fluorescence spectra were taken with a Horiba Jobin Yvon-Spex Fluorolog-3 fluorimeter. Quantum yield measurements are detailed in the Supporting Information.

Time-Resolved Measurements. Narrow band (line width = 6 nm), 150 fs pulses centered at 585 nm were used for the transient absorption spectroscopy. The spectrum was recorded using low-energy (<100 $\mu J/cm^2$) pumping pulses to avoid spurious effects and exciton−exciton annihilation in the TDBC J-aggregates.

■ ASSOCIATED CONTENT

Supporting Information

Additional details of the anticrossing of strongly coupled systems, transmission spectra simulated by transfer matrix formalism, fluorescence QY measurement, and transient absorption spectra. This material is available free of charge via the Internet at http://pubs.acs.org.

■ AUTHOR INFORMATION

Corresponding Author

*E-mail: ebbesen@unistra.fr.

Notes

The authors declare no competing financial interest.

■ ACKNOWLEDGMENTS

This work was partially supported by the ERC "Plasmonics" no. 22577, the ANR Equipex "Union" (ANR-10-EQPX-52-01), and the Labex NIE projects (ANR-11-LABX-0058_NIE) within the Investissement d'Avenir program ANR-10-IDEX-0002-02. We thank Chien-Wei Hsu for the absolute QY measurement and R. Voltz for reminding us of the long-lived excimers. S.W. acknowledges the personal support from the Chinese Scholarship Council (CSC).

■ REFERENCES

(1) Pockrand, I.; Brillante, A.; Möbius, D. Exciton−Surface Plasmon Coupling: An Experimental Investigation. *J. Phys. Chem.* **1982**, *77*, 6289−6295.

(2) Fujita, T.; Sato, Y.; Kuitani, T.; Ishihara, T. Tunable Polariton Absorption of Distributed Feedback Microcavities at Room Temperature. *Phys. Rev. B* **1998**, *57*, 12428−12434.

(3) Lidzey, D. G.; Bradley, D. D. C.; Skolnick, M. S.; Virgili, T.; Walker, S.; Whittaker, D. M. Strong Exciton−Photon Coupling in an Organic Semiconductor Microcavity. *Nature* **1998**, *395*, 53−55.

(4) Schouwink, P.; Berlepsch, H. V.; Dähne, L.; Mahrt, R. F. Dependence of Rabi-splitting on the Spatial Position of the Optically Active Layer in Organic Microcavities in the Strong Coupling Regime. *Chem. Phys.* **2002**, *285*, 113−120.

(5) Song, J. H.; He, Y.; Nurmikko, A. V.; Tischler, J.; Bulovic, V. Exciton-Polariton Dynamics in a Transparent Organic Semiconductor Microcavity. *Phys. Rev. B* **2004**, *69*, 235330.

(6) Wiederrecht, G. P.; Hall, J. E.; Bouhelier, A. Control of Molecular Energy Redistribution Pathways via Surface Plasmon Gating. *Phys. Rev. Lett.* **2007**, *98*, 083001.

(7) Virgili, T.; Coles, D.; Adawi, A. M.; Clark, C.; Michetti, P.; Rajendran, S. K.; Brida, D.; Polli, D.; Cerullo, G.; Lidzey, D. G. Ultrafast Polariton Relaxation Dynamics in an Organic Semiconductor Microcavity. *Phys. Rev. B* **2011**, *83*, 245309.

(8) Kéna-Cohen, S.; Forrest, S. R. Room-Temperature Polariton Lasing in an Organic Single-Crystal Microcavity. *Nat. Photonics* **2010**, *4*, 371−375.

(9) Plumhof, J. D.; Stöferle, T.; Mai, L.; Scherf, U.; Mahrt, R. F. Room-Temperature Bose−einstein Condensation of Cavity Exciton−Polaritons in a Polymer. *Nat. Mater.* **2014**, *13*, 247−252.

(10) Berrier, A.; Cools, R.; Arnold, C.; Offermans, P.; Crego-Calama, M.; Brongersma, S. H.; Gomez-Rivas, J. Active Control of the Strong Coupling Regime between Porphyrin Excitons and Surface Plasmon Polaritons. *ACS Nano* **2010**, *5*, 6226−6232.

(11) Schwartz, T.; Hutchison, J. A.; Genet, C.; Ebbesen, T. W. Reversible Switching of Ultrastrong Light-Molecule Coupling. *Phys. Rev. Lett.* **2011**, *106*, 196405.

(12) Hutchison, J. A.; Schwartz, T.; Genet, C.; Devaux, E.; Ebbesen, T. W. Modifying Chemical Landscapes by Coupling to Vacuum Fields. *Angew. Chem., Int. Ed.* **2012**, *51*, 1592−1596.

(13) Fontcuberta i Morral, A.; Stellacci, F. Light-Matter Interactions: Ultrastrong Routes to New Chemistry. *Nat. Mater.* **2012**, *11*, 272−273.

(14) Hayashi, S.; Ishigaki, Y.; Fujii, M. Plasmonic Effects on Strong Exciton-Photon Coupling in Metal-Insulator-Metal Microcavities. *Phys. Rev. B* **2012**, *86*, 045408.

(15) Schwartz, T.; Hutchison, J. A.; Léonard, J.; Genet, C.; Haacke, S.; Ebbesen, T. W. Polariton Dynamics under Strong Light−Molecule Coupling. *ChemPhysChem* **2013**, *14*, 125−131.

(16) Hutchison, J. A.; Liscio, A.; Schwartz, T.; Canaguier-Durand, A.; Genet, C.; Palermo, V.; Samorì, P.; Ebbesen, T. W. Tuning the Work-Function via Strong Coupling. *Adv. Mater.* **2013**, *25*, 2481−2485.

(17) Canaguier-Durand, A.; Devaux, E.; George, J.; Pang, Y.; Hutchison, J. A.; Schwartz, T.; Genet, C.; Wilhelms, N.; Lehn, J.-M.; Ebbesen, T. W. Thermodynamics of Molecules Strongly Coupled to the Vacuum Field. *Angew. Chem., Int. Ed.* **2013**, *52*, 10533−10536.

(18) Coles, D. M.; Grant, R. T.; Lidzey, D. G.; Clark, C.; Lagoudakis, P. G. Imaging the Polariton Relaxation Bottleneck in Strongly Coupled Organic Semiconductor Microcavities. *Phys. Rev. B* **2013**, *88*, 121303.

(19) Canaguier-Durand, A.; Genet, C.; Lambrecht, A.; Ebbesen, T. W.; Reynaud, S. Non-Markovian Polariton Dynamics in Organic Strong Coupling. arXiv:1307.8378 [cond-mat.mes-hall], 2013.

(20) Dintinger, J.; Klein, S.; Bustos, F.; Barnes, W. L.; Ebbesen, T. W. Strong Coupling between Surface Plasmon-Polaritons and Organic Molecules in Subwavelength Hole Arrays. *Phys. Rev. B* **2005**, *71*, 035424.

(21) Vasa, P.; Pomraenke, R.; Cirmi, G.; De Re, E.; Wang, W.; Schwieger, S.; Leipold, D.; Lienau, C. Ultrafast Manipulation of Strong Coupling in Metal− Molecular Aggregate Hybrid Nanostructures. *ACS Nano* **2010**, *42*, 7559−7565.

(22) Salomon, A.; Wang, S.; Hutchison, J. A.; Genet, C.; Ebbesen, T. W. Strong Light-Molecule Coupling on Plasmonic Arrays of Different Symmetry. *ChemPhysChem* **2013**, *14*, 1882−1886.

(23) Koponen, M. A.; Hohenester, U.; Hakala, T. K.; Toppari, J. J. Absence of Mutual Polariton Scattering for Strongly Coupled Surface Plasmon Polaritons and Dye Molecules with a Large Stokes Shift. *Phys. Rev. B* **2013**, *88*, 085425.

(24) Ni, W.; Yang, Z.; Chen, H.; Li, L.; Wang, J. Coupling between Molecular and Plasmonic Resonances in Freestanding Dye−Gold

Nanorod Hybrid Nanostructures. *J. Am. Chem. Soc.* **2008**, *130*, 6692−6693.
(25) Hao, Y.-W.; Wang, H.-Y.; Jiang, Y.; Chen, Q.-D.; Ueno, K.; Wang, W.-Q.; Misawa, H.; Sun, H.-B. Hybrid-State Dynamics of Gold Nanorods/Dye J-Aggregates under Strong Coupling. *Angew. Chem., Int. Ed.* **2011**, *123*, 7970−7974.
(26) Gómez, D. E.; Lo, S. S.; Davis, T. J.; Hartland, G. V. Picosecond Kinetics of Strongly Coupled Excitons and Surface Plasmon Polaritons. *J. Phys. Chem. B* **2012**, *117*, 4340−4346.
(27) Zengin, G.; Johansson, G.; Johansson, P.; Antosiewicz, T. J.; Käll, M.; Shegai, T. Approaching the Strong Coupling Limit in Single Plasmonic Nanorods Interacting with J-aggregates. *Sci. Rep.* **2013**, *3*, 3074.
(28) Nagasawa, F.; Takase, M.; Murakoshi, K. Raman Enhancement via Polariton States Produced by Strong Coupling between a Localized Surface Plasmon and Dye Excitons at Metal Nanogaps. *J. Phys. Chem. Lett.* **2014**, *5*, 14−19.
(29) Zhu, Y.; Gauthier, D. J.; Morin, S. E.; Wu, Q.; Carmichael, H. J.; Mossberg, T. W. Vacuum Rabi Splitting as a Feature of Linear-Dispersion Theory: Analysis and Experimental Observations. *Phys. Rev. Lett.* **1990**, *64*, 2499−2502.
(30) Birks, J. B. *Photophysics of Aromatic Molecules*; Wiley-Interscience: New York, 1970.
(31) Makio, S.; Kanamaru, N.; Tanaka, J. The J-Aggregate 5,5′,6,6′-Tetrachloto-1-1′-diethyl-3,3′-bis(4-sulfobutyl)-benzimidaolecarbocyanine Sodium Salt in Aqueous Solution. *Bull. Chem. Soc. Jpn.* **1980**, *53*, 3120−3124.
(32) Agranovich, V. M.; Litinskaia, M.; Lidzey, D. G. Cavity Polaritons in Microcavities Containing Disordered Organic Semiconductors. *Phys. Rev. B* **2003**, *67*, 085311.
(33) Andric, G.; Boas, J. F.; Bond, A. M.; Fallon, G. D.; Ghiggino, K. P.; Hogan, C. F.; Hutchison, J. A.; Lee, M. A.-P; Langford, S. J.; Pilbrow, J. R.; Troup, G. J.; Woodward, C. P. Spectroscopy of Naphthalene Diimides and Their Anion Radicals. *Aust. J. Chem.* **2004**, *57*, 1011−1019.
(34) Decher, G. Fuzzy Nanoassemblies: Toward Layered Polymeric Multicomposites. *Science* **1997**, *277*, 1232−1237.
(35) Bradley, M. S.; Tischler, J. R.; Bulović, V. Layer-by-Layer J-Aggregate Thin Films with a Peak Absorption Constant of 10^6 cm^{-1}. *Adv. Mater.* **2005**, *17*, 1881−1886.
(36) Muenter, A. A.; Brumbaugh, D. V.; Apolito, J.; Horn, L. A.; Spano, F. C.; Mukamel, S. Size Dependence of Excited-State Dynamics for J-Aggregates at Silver Bromide Interfaces. *J. Phys. Chem.* **1992**, *96*, 2783−2790.
(37) Reid, P. J.; Higgins, D. A.; Barbara, P. F. Environment-Dependent Photophysics of Polymer-Bound J Aggregates Determined by Time-Resolved Fluorescence Spectroscopy and Time-Resolved near-Field Scanning Optical Microscopy. *J. Phys. Chem.* **1996**, *100*, 3892−3899.